

S. aureus Abscess Development in a Murine Model Measured using MR Relaxometry and Diffusion Tensor Imaging

M. D. Boska¹, M. Uberti¹, A. Aldrich², E. McIntyre¹, and T. Kielian²

¹Radiology, University of Nebraska Medical Center, Omaha, NE, United States, ²Pathology and Microbiology, University of Nebraska Medical Center, Omaha, NE, United States

Introduction. Brain abscesses develop in response to a parenchymal infection with pyogenic bacteria, beginning as a localized area of cerebritis and evolving into a suppurative lesion surrounded by a well-vascularized fibrotic capsule¹. Despite recent advances made in detection and therapy, brain abscess remains a serious CNS infectious disease that can lead to long-term complications including seizures, loss of mental acuity, and focal neurological defects that are lesion site-dependent. The most common etiologic agents of brain abscess are the *streptococcal* strains and *Staphylococcus aureus* (*S. aureus*)². Based upon its prevalence in human CNS infection, our laboratory has utilized *S. aureus* to establish an experimental brain abscess model in the mouse that accurately reflects the course of disease progression in humans^{3,4}, providing an excellent model system to characterize changes during brain infection using MRI modalities.

Methods. *Animals and Lesion Induction.* Female C57BL/6 mice were purchased from the National Cancer Institute (Rockville, MD) and used at 6-8 weeks of age. Brain abscesses were induced by stereotactic inoculation of live *S. aureus* into the caudate/putamen region of the brain as previously described⁵. Mice were anesthetized by inhalation of 1% isoflurane in a nitrous oxide/oxygen mixture prior to MRI data acquisition. All animal procedures were in accordance with National Institutes of Health guidelines and were approved by the Institutional Animal Care and Use Committee of the University of Nebraska Medical Center. Quantitative magnetic resonance imaging (MRI) was performed on sham operated animals and *S. aureus*-infected mice at days 3, 7, 10 and 14 after infection. Quantitative MRI included T_1 mapping, T_2 mapping, and diffusion tensor imaging (DTI). *Lesion metrics.* T_1 , T_2 , and DTI metrics fractional anisotropy (FA) and mean diffusivity (D_{av}) were used to segment the lesion and lesion wall and measure relative to similar brain regions in controls. *Magnetic Resonance Imaging.* MRI data were obtained using a Bruker Avance 7 Tesla/21 cm system operating at 300.41 MHz using actively decoupled 72 mm volume coil transmit and a laboratory built 1.25 x 1.5 cm receive surface coil. T_1 maps were generated using a progressive saturation multislice spin echo sequence with TE=10 ms and TR=10, 5, 2, 1.5, 1, 0.8, 0.6 and 0.4 s with 25 interleaved contiguous slices, slice thickness of 0.5 mm, 20 mm FOV, 96 x 128 resolution acquired in 10 min. T_2 maps were generated using a CPMG phase cycled multiecho sequence with TR = 4500 ms and TE = 10, 20, 30, 40, 50, 60, 70, and 80 ms, 20 mm FOV, 0.5 mm slice thickness and 256 x 196 in plane resolution acquired in 12 minutes. DTI data were acquired using a single-shot diffusion-weighted spin-echo planar imaging (TE=42 ms) with respiratory gating to prevent motion artifacts T_R =10-15 s, depending on respiratory rate. EPI acquisition parameters included 15 slices, 200 KHz bandwidth, 96 X 96 in plane acquisition zero-filled to 256 X 256, and a 0.5 mm slice thickness. The diffusion encoding used is a balanced, rotationally-invariant and alternating polarity icosahedral scheme (12 directions)^{6,7}. The encoding scheme was designed to reduce background-diffusion gradient couplings⁸. Diffusion weighting b-factor = 800 s mm⁻², δ =4ms, Δ =15ms, G_{dmax} = 40 G/cm, 200 μ s rise time, 7 averages for $b=0$ acquisition, 7 averages for each $b=800$ encoding direction, for a total acquisition time of 15-30 min, depending upon respiration rate. *Data Analyses.* Analysis of the diffusion-weighted data was performed using custom programs written in IDL as previously described^{6,9}. Analysis produced maps of the three primary eigenvectors of diffusivity ($\lambda_1, \lambda_2, \lambda_3$), average diffusivity (D_{av}) where: $D_{av} = 1/3 * (\lambda_1 + \lambda_2 + \lambda_3)$ and fractional anisotropy (FA).

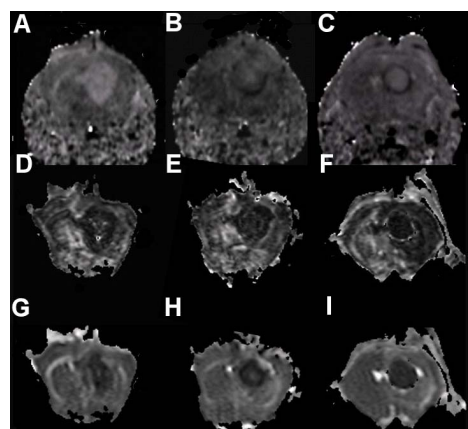


Figure 1 Time course of the central slice of the brain showing (A-C) T_1 map, (D-F) FA map and (G-I) D_{av} at days (A,D,G) 3, (B,E,H) 7 and (C,F,I) 14.

network of myofibroblasts and the deposition of extracellular matrix components including fibronectin and collagen¹. The T_1 of the abscess was increased initially to 843 ± 7 ms at day 3 and progressively decreased to 763 ± 14 ms at day 14. However, the T_1 of the wall was decreased relative to normal brain (740 ± 12 ms) and decreased from 714 ± 13 ms at day 7 to 704 ± 8 ms at day 14. Over time the abscess cavity regressed in size, which may be attributed to the contractile nature of myofibroblasts. In addition, FA and D_{av} were significantly decreased in the abscess compared to normal brain. The T_2 of both the abscess and the wall were increased relative to normal brain (White matter $T_2 = 46 \pm 0.7$ ms). Wall T_2 decreased from 71 ± 2 ms at day 7 to 64 ± 2 ms at day 14. The abscess T_2 reduced from 80 ± 2 ms at day 3 to 71 ± 2 ms at day 14. Work to correlate T_1 , T_2 , FA, D_{av} and individual diffusion eigenvalues with histology is currently in progress.

Conclusion. This report represents the first MRI work on an animal model of brain abscess characterizing the MR signatures during lesion development. These works and correspondence with histology will be used for assessing the kinetics and effects of experimental therapies in this disease model.

Acknowledgements. This work was supported by NIH: 1 P01 NS043985-01, 5 P01, MH64570-03, P20 RR15635 (MB), and 2RO1 NS40730 (T.K.) **References.** 1. Kielian, T., *J. Neuroinflammation* 1, 1-16 (2004). 2. Mathisen, G. E., and J. P. Johnson., *Clin Infect Dis* 25, 763-779 (1997). 3. Kielian, T., Haney, A., Mayes, P.M., Garg, S., and Esen N., *Immunol* 73, 7428-7435 (2005). 4. Kielian, T., Syed, M.Md, Liu, S., Phillips, N., Wagoner, G., Drew, P.D., and Esen, N. J. *Immunol* 180, 5004-5016 (2008). 5. Kielian, T., Phulwani, N.K., Esen, N., Syed, M., Haney, A.C., McCastlain, K., and Johnson J. *J. Immunol* 178, 4528-4537 (2007). 6. Hasan, K.M., Bassar, P.J., Parker, D.L. & Alexander, A.L. *J Magn Reson* 152, 41-7 (2001). 7. Hasan, K.M., Parker, D.L. & Alexander, A.L. *J Magn Reson Imaging* 13, 769-80 (2001). 8. Neeman, M., Freyer, J.P. & Sillerud, L.O. *Magn Reson Med* 21, 138-43 (1991). 9. Bassar, P.J., Mattiello, J. & LeBihan, D. *J Magn Reson B* 103, 247-54 (1994).